Optical source profiles of brown carbon in size-resolved particulate matter from typical domestic biofuel burning over Guanzhong Plain, China

Yali Lei [a,b], Zhenxing Shen [a,b,*], Tian Zhang [a], Qian Zhang [a], Qiyuan Wang [b], Jian Sun [a], Xuesong Gong [a], Junji Cao [b], Hongmei Xu [a], Suixin Liu [b], Liu Yang [a]

[a] Department of Environmental Science and Engineering, Xi'an Jiaotong University, Xi'an 710049, China
[b] Key Lab of Aerosol Chemistry & Physics, Institute of Earth Environment, Chinese Academy of Sciences, Xi'an 710049, China

HIGHLIGHTS

- Optical profiles of BrC in size-resolved PM from biomass burning were investigated.
- Different size distribution pattern of BrC optical properties were found between "heated kang" and the advance stove.
- The advanced stove was effective on BrC emission reduction compared to "heated kang".

GRAPHICAL ABSTRACT

Simple forcing efficiency of MSOC at UV region (300–400 nm) from $PM_{2.5}$ biomass burning under different combustion conditions.
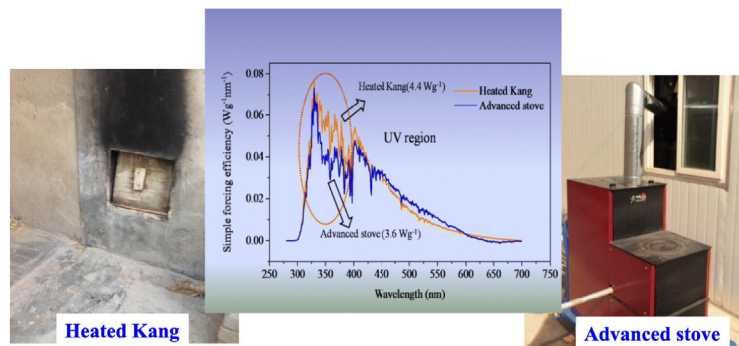
ARTICLE INFO

ABSTRACT

In this study, both $PM_{2.5}$ and size-resolved source samples were collected from a "heated kang" and an advanced stove to investigate the optical properties of brown carbon (BrC). The light-absorption coefficient (b_{abs}), the absorption Ångström exponent (AAE), and the mass absorption cross-section (MAC) of both water and methanol-extracted BrC were investigated. The methanol-extracted BrC ($BrC_{methanol}$) had higher light absorption than water-extracted BrC (BrC_{water}). The value of $PM_{2.5}$ b_{abs} of $BrC_{methanol}$ at 365 nm ($b_{abs365,methanol}$) dramatically decreased from 64,669.8 Mm^{-1} for straw burning in the "heated kang" to 1169.2 Mm^{-1} for maize straw briquettes burning in the advanced stove at the same burning rate. The value of $PM_{2.5}$ MAC for $BrC_{methanol}$ at 365 nm ($MAC_{365,methanol}$) decreased from 1.8 $m^2\,g^{-1}$ in the "heated kang" to 1.3 $m^2\,g^{-1}$ in the advanced stove. For smoldering burning in the "heated kang", $b_{abs365,methanol}$, $MAC_{365,methanol}$, and K^+ showed a unimodal distribution that peaked at sizes <0.4 μm. However, the $b_{abs365,methanol}$ and $MAC_{365,methanol}$ size distributions of the briquette burning in the advanced stove showed a bimodal pattern, with a large peak at sizes <0.4 μm and a minor peak in the size range of 4.7–5.8 μm. The $b_{abs365,methanol}$ value for sizes <0.4 μm (277.4 Mm^{-1}) was only 12.3% compared to those obtained from the "heated kang". The burning rate did not influence the size distribution pattern of either the "heated kang" or the advanced stove. Results from a radiative model show that biomass burning is an

important factor for light absorptivity, and the use of an advanced stove can reduce the simple forcing efficiency value by nearly 20% in UV bands compared to the "heated kang". Our results indicate that changing the combustion style from maize straw smoldering to briquette burning in an advanced stove can effectively reduce BrC emissions during heating seasons in rural areas of Guanzhong Plain.

1. Introduction

Light-absorbing organic compounds (i.e., brown carbon, BrC) play an important, yet poorly understood, role in the planetary radiation budget and global climate change (Lambe et al., 2013; Laskin et al., 2015; Liu et al., 2013; Washenfelder et al., 2015; Zhao et al., 2015). A recent study argued that previous models overestimated the radiative forcing of black carbon (BC) due to the incorrect attribution of BrC absorption to BC (Wang et al., 2014). Previous modeling studies reported that BrC contributes 0.1 to 0.25 W m^{-2} to the global radiative forcing (Feng et al., 2013). Chen and Bond (2010) reported that the contribution of BrC could be important in energy balances over bright surfaces using a simple forcing efficiency (SFE). Calculations using the aerosol optical depth have determined that the contribution of BrC to the total carbonaceous aerosol absorption was 28% at 440 nm in California (Bahadur et al., 2012) and 20% at 550 nm globally (Chung et al., 2012). Poschl (2003) suggested that BrC such as polycyclic aromatic hydrocarbons, PAHs, humic-like substances, HULIS and biopolymers can impact human health.

Field observations and laboratory studies have shown that particles emitted from the incomplete and/or smoldering combustion of biomass (Hoffer et al., 2006; Lack et al., 2012), fossil fuels (Kirchstetter et al., 2004), biological aerosols (Andreae and Gelencser, 2006), contain substantial amounts of BrC. There is also laboratory evidence that shows that BrC is produced from a variety of chemical processes (Lambe et al., 2013). Previous studies have reported that the contribution of biomass burning to light absorption was 35%–50% at 300 nm in Amazonia (Hoffer et al., 2006) and 30%–40% at 400 nm in Xianghe, China (Yang et al., 2009), indicating that emission produced by biomass burning plays a significant role in light absorption. Shen et al. (2017a) verified that BrC was emitted from biomass burning and coal burning in rural Xi'an, suggesting that the coal-burning absorption Ångström exponent (AAE; with a value of 4.38) was much smaller than those for biomass subjected to smoldering burning (7.44) and straw pellet burning (6.78). Yan et al. (2015) showed that biomass burning contributed 17 ± 4% (winter) and 19 ± 5% (summer) of the total water-soluble organic carbon (WSOC) light absorption in Beijing. However, the light-absorption contributions of BrC from biomass burning, and its microphysical properties such as size distributions, optical properties and the mixing state of biomass burning particles, have not yet been chemically qualified.

Biomass burning plays an important role in winter PM pollution over Xi'an (Cao et al., 2005; Shen et al., 2008, 2009; Zhang et al., 2014; Zhu et al., 2016). For example, Zhang et al. (2014) suggested that biomass burning contributed 5.1%–43.8% of the total OC in Xi'an. The traditional method of domestic heating during winter in this area is straw smoldering in a "heated kang", which causes serious problems to rural and urban air quality (Sun et al., 2017). In this study, the optical source profiles of BrC in size-resolved particulate matter from biomass burning are measured. The purposes of this study are: (1) to compare the optical properties between water-extracted and methanol-extracted BrC; (2) to investigate the optical sources profiles of size-resolved particulate matter obtained from biomass burning; and (3) to compare the light absorption and radiative forcing of BrC between straw smoldering in a "heated kang" and maize straw briquettes burned in an advanced type of stove.

2. Methodology

2.1. Sampling measurements

The on-site residential burning experiment was conducted in a house where maize straw smoldering in a "heated kang" had been used for heating during the winter for many years. An advanced stove with an automatic fuel-feeding system was also set up in a laboratory combustion chamber to simulate residential heating activities, at the Institute of Earth Environment, Chinese Academy of Sciences in collaboration with the Desert Research Institute, USA. The combustion was equipped with a thermocouple, a thermos-anemometer, an air-purification system and a sampling line connected to a dilution sampler. Source samples were collected for typically 1–2 h using a custom-made dilution system with an adjustable dilution rate of 5- to 15-fold. PM$_{2.5}$ samples were collected with a quartz-fiber filter from three parallel channels located downstream of the residence chamber, which had a flow rate of 5 L min^{-1} per channel (Fig. S1). Detailed description of smoldering in a "heated kang" and advanced stove combustion can be found in Sun et al. (2017). In addition, size-resolved particle samples were collected with a pre-combusted (450 °C, 6 h) quartz fiber filter (Whatman, Φ 80 mm) with size cuts of 0.4, 0.7, 1.1, 2.1, 3.3, 4.7, 5.8, and 9.0 μm, at a flow rate of 28.3 L min^{-1} using an eight-stage cascade impactor (Anderson, Thermo Fisher Scientific, Franklin, MA, USA). Field blanks were collected before and after the sampling by mounting the filter onto the three types of samplers for 10 min without sucking any air (Wang et al., 2011). After sampling, the exposed filters were placed in clean plastic cassettes and stored in a refrigerator at ~4 °C until analysis to minimize any evaporation of volatile components. The PM samples were equilibrated using controlled temperature (20 °C–23 °C) and relative humidity (355–45%) desiccators for 24 h before and after sampling, and their mass loadings were determined gravimetrically using a Sartorius MC5 electronic microbalance (±1 μg sensitivity; Sartorius, Göttingen, Germany). Each filter was weighed at least three times before and after sampling following the 24 h equilibration period. The differences among the three repeated weightings were typically <10 μg for the blanks, and 15 μg for the sample filters.

2.2. Chemical analysis

The organic carbon (OC) and elemental carbon (EC) in the filter samples were studied with a DRI Model 2001 Thermal/Optical Carbon Analyzer (Atmoslytic Inc., Calabasas, CA, USA). The IMPROVE_A (Interagency Monitoring of Protected Visual Environments) protocol produces four OC fractions (OC1, OC2, OC3, and OC4 at 140 °C, 180 °C, 480 °C, and 580 °C, respectively, in a 100% He atmosphere), the pyrolyzed carbon fraction (OP, determined when reflected or transmitted laser light attained its original intensity after O$_2$ was added to the analysis atmosphere), and three EC fractions (EC1, EC2, and EC3 in a 98% He/2% O$_2$ atmosphere at 580 °C, 740 °C, 840 °C, respectively). OC was defined as OC1 + OC2 + OC3 + OC4 + OP and EC as EC1 + EC2 + EC3-OP (Chow et al., 2004). One replicate analysis was performed for each of the 10 samples. Details of the quality assurance and control procedures are described in Cao et al. (2003). One-fourth of each filter sample was dissolved in distilled-deionized water (10 mL) with a resistivity of 18.3 MΩ for a separate analysis of the water-soluble ions. Water-

soluble K^+ was analyzed with ion chromatography (Dionex 500, Dionex Corp, Sunnyvale, CA, USA). Detailed description of the ionic analysis can be found in Shen et al. (2008).

2.3. Optical properties of aerosol extracts

Two punches of filters taken from biomass burning $PM_{2.5}$ samples were extracted in 50 mL methanol (HPLC Grade, 99.9%, Fisher Scientific, NH, USA) and ultrapure water (with a sensitivity of 18.3 MΩ), by 30 min of sonication. For the size-resolved samples, one-fourth of each filtered sample were extracted in 50 mL methanol and ultrapure water. All extracts were filtered 1–3 times with a 25 mm diameter, 0.45 μm pore-size microporous membrane (Puradisc 25 TF, PTFE membrane). The light-absorption spectra of the methanol and water extracts were measured with a UV–Vis spectrophotometer (UV-6100s, MAPADA, Shanghai, China) with 10 cm optical paths in the individual solvent. Each spectrum was determined relative to a reference cuvette which contained the same solvent. Although light-absorption spectra were recorded from 200–1100 nm, signals <300 nm and >700 nm were not include in this study for substantial noise influence.

Aerosol absorption spectra of the methanol extracts (which represent the bulk amount of methanol-soluble organic carbon) were used to assess the light absorption coefficient (b_{abs}), as described by Liu et al. (2013) and Srinivas and Sarin (2014). The value of b_{abs} was calculated according to:

$$b_{abs\ \lambda,water/methanol} = (A_{\lambda,water/methanol} - A_{700,water/methanol}) * (V_{ext} * Portions) * \ln(10)/(V_{aero} * L) \quad (1)$$

where b_{abs} is expressed in units of Mm^{-1} (or $10^{-6}\ m^{-1}$). A_λ and A_{700} correspond to the measured absorbance at a specific λ and 700 nm, respectively. V_{ext} refers to the volume of the aqueous extract (50 mL) in which different portions of filter. V_{aero} corresponds to the sampling volume, and L is the path length of the cell (10 cm). We used the absorbance at 365 nm to estimate b_{abs} of the light-absorbing methanol-soluble organic carbon (also referred as BrC) (Liu et al., 2013). This wavelength was chosen since it is far enough from the UV region to avoid interferences from non-organic compounds (e.g., nitrates) (Lukacs et al., 2007).

The relationship between the wavelength-dependent AAE and b_{abs} of BrC in aqueous extracts is described following Hecobian et al. (2010):

$$b_{abs\ \lambda,water/methanol} = K * \lambda^{-AAE\ water/methanol} \quad (2)$$

Here, K refers to a constant value, and λ denotes the wavelength of the BrC. In this study, AAE is calculated by a linear-regression fit to $\log(b_{abs})$ vs. $\log(\lambda)$ in the wavelength range 300–500 nm.

For the methanol extracts, only light-absorption spectra were analyzed since the use of an organic solvent prohibits determining the carbon mass in these solutions. As a consequence, the mass-absorption cross-section (MAC) of BrC ($m^2\ g^{-1}$) at 365 nm was calculated based on the following equation (Zhang et al., 2013):

$$MAC_{\lambda,methanol} = b_{abs\ \lambda,methanol}/OC \quad (3)$$

2.4. Radiative effect calculation

In this study, the simple forcing efficiency (SFE, W g^{-1}) introduced by Bond and Bergstrom (2006) is used to estimate the direct radiative effect of biomass burning. SFE was originally normalized for the particle masses reported by Chylek and Wong (1995). A wavelength-dependent version that can be integrated to produce the total forcing is as follows:

$$\frac{dSFE}{d\lambda} = -\frac{1}{4}\frac{dS(\lambda)}{\lambda}\tau^2_{atm}(\lambda) \cdot (1 - F_c) \times \left[2(1-a_s)^2 \cdot \beta(\lambda) \cdot MSC(\lambda) - 4a_s MAC(\lambda)\right] \quad (4)$$

where $dS(\lambda)/d(\lambda)$ is the solar irradiance based on the ASTM G173-03 Reference Spectra, τ_{atm} is the atmospheric transmission (0.79), F_c is the cloud fraction (0.6), and a_s is the surface albedo (0.19). $\beta(\lambda)$ is the backscatter fraction, which is estimated with a quadratic polynomial, $\beta = 0.0817 + 1.8495b - 2.9682b^2$, where b is the atmospheric backscatter fraction calculated from the ratio of the backscattering mass cross sections to the total scattering (MSC_{back}/MSC). MAC is the mass absorption cross section. In this study, only absorption is considered. We performed Mie calculations every 1 nm between 280 and 700 nm to provide the MAC. Eq. (4) was thus simplified to:

$$\frac{dSFE}{d\lambda} = a_s \cdot \tau^2_{atm}(\lambda) \cdot (1 - F_c) \cdot MAC(\lambda)\frac{dS(\lambda)}{\lambda} \quad (5)$$

3. Results and discussion

3.1. Absorption spectra of water and the methanol extracts

To better evaluate the light absorption of BrC, the bulk solution properties of both the water and methanol extracts from the biomass burning source samples were first analyzed using the same UV–Vis spectrophotometer. Fig. 1 shows a typical absorption spectra of water and the methanol extracts from the selected samples for both the smoldering and flaming biomass burning, respectively. The absorption for both the methanol and water extracts are highly correlated with wavelength. It is found that the methanol extracts had higher light absorption than the water-extracts across all wavelengths from 300 to 700 nm. Table 1 compares the light-absorbing properties between the water and methanol extracts for the $PM_{2.5}$ biomass burning source samples emitted from a "heated kang" and an advanced stove at different wavelengths (340, 365, 450, and 570 nm). From our data, the water/methanol ratios of b_{abs365} for the "heated kang" and the advanced stove were 0.5 and 0.6, respectively. The results indicate that light absorption of BrC was underestimated greatly by the water extracts when compared with the methanol extracts. Therefore, water-insoluble OC (WIOC) was important when evaluating the OC light absorption. Zhang et al. (2013) also reported that b_{abs} of WIOC ranged from 16% to 80% of $b_{abs365,methanol}$.

The AAE values (fitted from 300 to 500 nm) of the methanol and water extracts BrC were quite different. The $AAE_{methanol}$ values (fitted from 300 to 500 nm) were similar for the smoldering and flaming biomass burning. However, AAE_{water} showed some differences, indicating that the light absorbing substance of BrC_{water} between the smoldering and flaming combustion varies to some extent. The AAE_{water} values have a mean of 6.1 ± 1.2 according to Table 1, which are in the same range of the biomass smoke aerosol reported by Kirchstetter et al. (2004), but much lower than the wood combustion values (13.2 ± 3.1) reported by Chen and Bond (2010). In contrast, the $AAE_{methanol}$ values were on average 5.9 ± 0.6, which are a little lower than the average AAE_{water} value found in this study, but higher than the atmospheric aerosol samples (4.8 ± 0.5) obtained in the Los Angeles Basin by Zhang et al. (2013).

3.2. Smoldering straw in "heated kang"

As shown in Table 2, the value of $b_{abs365,methanol}$ for straw smoldering, with a burning rate of 1 kg h^{-1} in the "heated kang", showed a strong absorbance of 64,669.8 Mm^{-1}. The typical $AAE_{methanol}$ value fitted from 300 to 500 nm was 6.7, which was a little lower than that
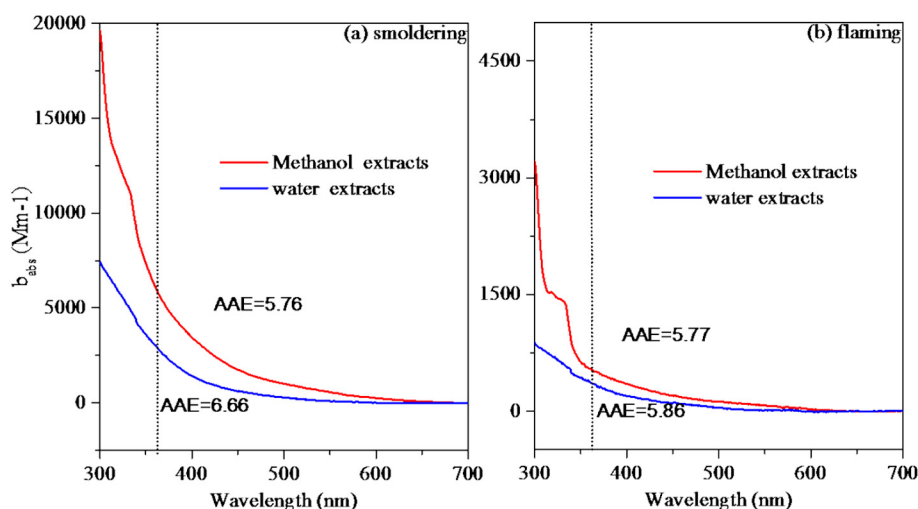
Fig. 1. Water and methanol extracts from the selected smoldering and flaming biomass burning samples. AAE is calculated by linear regression fit to log b_{abs} & log λ in the wavelength between 300–500 nm.

in the ambient winter $PM_{2.5}$ values in Beijing (7.1, Cheng et al., 2016) and Xi'an (7.24, Shen et al., 2017b), which both demonstrated that biomass burning was an important source of $BrC_{methanol}$. Normalizing $b_{abs365,methanol}$ (without interfering absorbance by EC and inorganics) to the OC mass yields $MAC_{365,methanol}$ characterizes the absorbing efficiency of BrC. The $MAC_{365,methanol}$ value for smoldering straw in the "heated kang" was 1.8 $m^2 g^{-1}$, similar to that emitted from wood burning (~1.85 $m^2 g^{-1}$) reported by Chen and Bond (2010), but higher than that of winter $PM_{2.5}$ in Beijing (1.45 $m^2 g^{-1}$, Cheng et al., 2016) and Xi'an (1.46 $m^2 g^{-1}$, Shen et al., 2017b), and much higher than that of summer $PM_{2.5}$ in Xi'an (0.59 $m^2 g^{-1}$, Shen et al., 2017b). This is because winter $PM_{2.5}$ $BrC_{methanol}$ in Xi'an mainly arises from biomass burning and coal burning to produce heat, and fresh secondary organic carbon (SOC) from aqueous heterogeneous reactions, while summer $PM_{2.5}$ $BrC_{methanol}$ is produced by vehicle emissions and fresh and aged SOC in photochemical processes (Shen et al., 2017b). Thus, we can infer that $BrC_{methanol}$ from biomass burning tends to be more light-absorbing than those associated with vehicle emissions, coal combustion, and SOC formation. Additionally we can see that the largest influencing factor on light absorption at different combustion conditions was associated with air supply (Table 2). Maize straw burning in a "heated kang" is generally limited the oxygen supply to extend the combustion time.

The size distributions of the individual species, including OC, water-soluble K, $b_{abs365,methanol}$ and $MAC_{365,methanol}$ for smoldering straw with

different burning rates (1.0 kg h^{-1} and 2.0 kg h^{-1}) in the "heated kang" are shown in Fig. 2. The values of $b_{abs365,methanol}$ mostly exist in the fine mode (<2.1 μm), and, on average, they account for 96.6% of the whole particle matters size. It was clear that $b_{abs365,methanol}$ and $MAC_{365,methanol}$ show a unimodal size distribution, with a large peak for sizes <0.4 μm. The $b_{abs365,methanol}$ values for sizes <0.4 μm (4015.3 ± 2509.1 Mm^{-1} on average) accounted for 41.5% of the sub-micron particles (<1.1 μm, 9343.7 ± 4751.2 Mm^{-1}) and 39.8% in the fine mode (<2.1 μm, 9720.1 ± 4824.0 Mm^{-1}), respectively. However, the OC in the fine mode tended to be larger, peaking in the 0.4–0.7 μm range. The OC exhibited a different size distribution pattern compared to $b_{abs365,methanol}$. OC levels in the size range 0.4–0.7 μm were ~1.7 times larger than those with sizes <0.4 μm. It can be inferred that BrC produced from biomass burning is more concentrated in finer particles.

Interestingly, it is noted that different burning rates produced similar size distribution patterns for $BrC_{methanol}$ produced by the "heated kang" (Fig. 2), but the optical properties values showed some difference. For example, the $b_{abs365,methanol}$ value (<0.4 μm) for a burning rate of 2 kg h^{-1} was 5789.5 Mm^{-1}, which is dramatically lower than the value 2241.1 Mm^{-1} obtained for the 1.0 kg h^{-1} rate. The $MAC_{365,methanol}$ value (<0.4 μm) from the burning rate of 2 kg h^{-1} was 1.3 $m^2 g^{-1}$, which was 1.3 times larger than that obtained with a burning rate of 1 kg h^{-1}. Such a phenomenon illustrates that a faster burning rate may lead to more emission of finer $BrC_{methanol}$ particles, as mentioned above. Liu et al. (2013) reported that $b_{abs365,methanol}$ for ambient aerosol (in Atlanta, USA) also showed a unimodal size distribution, with a large peak in the size ~0.5 μm, while the pure HULIS particles reported by Hoffer et al. (2006) had a light absorption peak in the size range 0.5–0.6 μm. Therefore, $BrC_{methanol}$ produced from smoldering straw biomass burning peaks at finer size than ambient aerosol and pure HULIS particles.

3.3. Briquette burning in an advanced stove

An advanced stove with an automatic fuel feeding system was installed in the chamber to evaluate any PM reduction in comparison with the "heated kang" (Sun et al., 2017). In this study, the optical properties of particles created from this advanced stove were investigated and compared with those obtained from the "heated kang". The $b_{abs365,methanol}$ value of $PM_{2.5}$ $BrC_{methanol}$ from straw burning in the "heated kang" decreased by >90% in comparison with the briquette burning in the advanced stove at the same burning rate (1 kg h^{-1}) (Table 2). The value of $PM_{2.5}$ $MAC_{365,methanol}$ varied from 0.71 $m^2 g^{-1}$ to 1.75 $m^2 g^{-1}$, with an average of 1.3 ± 0.3 $m^2 g^{-1}$, which is lower than that obtained with the "heated kang" (1.8 $m^2 g^{-1}$). It is noted

Table 1
Values of b_{abs}, AAE, and the ratios between water and methanol extracts for $PM_{2.5}$ samples in the "heated kang" and advanced stove.

	$b_{abs\ water}$				AAE_{water}
	340 nm	365 nm	450 nm	570 nm	300–500 nm
Heated kang	67,507.8	35,599.2	4385.8	264.8	9.5
Advanced stove	1496.2	1034.5	259.1	31.3	6.2
	$b_{abs\ methanol}$				$AAE_{methanol}$
	340 nm	365 nm	450 nm	570 nm	300–500 nm
Heated kang	103,593.6	64,669.8	15,843.7	2666.0	6.7
Advanced stove	2916.1	1766.5	596.1	135.7	5.9
	$b_{abs\ water}/b_{abs\ methanol}$				$AAE_{water}/AAE_{methanol}$
	340 nm	365 nm	450 nm	570 nm	300–500 nm
Heated kang	0.6	0.5	0.3	0.1	0.7
Advanced stove	0.5	0.6	0.4	0.2	0.9

Table 2

Comparison of $b_{abs365,methanol}$, $AAE_{methanol}$, $MAC_{365,methanol}$ of $PM_{2.5}$ BrC under different burning conditions of the experiments in this study.

Test	Fuel type	Type of stove	$b_{abs365,methanol}$ Mm^{-1}	$AAE_{methanol}$ 300–500 nm	$MAC_{365,methanol}$ m^2 g^{-1}	MCE %	Burning rate, kg h^{-1}
1	Maize straw-1 kg	Heated kang smoldering	64,669.8	6.7	1.8	–	1
2	Maize residue briquette-1 kg	Advanced stove smoldering + flaming	1360.4	5.8	1.5	81.5	1.2
	Maize residue briquette-1 kg	Advanced stove smoldering + flaming	1169.2	7.2	0.7	90.9	1
3	Maize residue briquette-3 kg	Advanced stove smoldering + flaming	5640.3	5.8	1.3	81.3	1.2
	Maize residue briquette-3 kg	Advanced stove smoldering + flaming	2081.5	6.3	1.1	90.2	1
4	Maize residue briquette-1 kg	Advanced stove flaming only	810.1	5.4	1.5	93.5	1.2
	Maize residue briquette-1 kg	Advanced stove flaming only	504.8	5.3	1.2	95.4	1
5	Maize residue briquette-3 kg	Advanced stove flaming only	1676.9	5.9	1.1	93.5	1.2
	Maize residue briquette-3 kg	Advanced stove flaming only	888.7	5.8	1.8	95.9	1

that the burning rate had very little influenced on $AAE_{methanol}$, but higher burning rates led to higher $b_{abs365,methanol}$. For example, the average $b_{abs365,methanol}$ at a burning rate of 1.2 kg h^{-1} was two times larger than that for a burning rate of 1 kg h^{-1}. It is inferred that a faster burning rate can deplete the oxygen supply and then lead to higher $BrC_{methanol}$ emission. Sun et al. (2017) reported that a higher burning rate usually led to a lower modified combustion efficiency (MCE), but high PM emission factors (Sun et al., 2017). High PM emission resulted in high BrC productions (Sun et al., 2017). MCE is another variable that can influence BrC emission. In this study, the calculation of MCE is shown as follows:

$$MCE = \frac{\Delta[CO_2]}{\Delta[CO] + \Delta[CO_2]} \qquad (6)$$

where $\Delta[CO]$ and $\Delta[CO_2]$ are the excess molar mixing-ratios of CO and CO_2, respectively. A higher burning rate usually led to lower MCE, but

high PM emission factors (Sun et al., 2017). Normally, MCE values <90% are defined as smoldering combustion; otherwise it was flaming combustion (Andreae and Merlet, 2001; Oanh et al., 2011; Shen et al., 2011). Much higher MCE values produced the advanced stoves was also compared to those obtained from the "heated kang" (Sun et al., 2017). As discussed earlier, advanced stoves with low burning rates and high MCEs can be an effective means for reducing PM and BrC emission in rural areas of the Guanzhong Plain.

The size distribution patterns of $b_{abs365,methanol}$ and $MAC_{365,methanol}$ for straw briquettes burning in the advanced stove display a bimodal size distribution with a major peak for sizes <0.4 μm and a minor peak in the size range 4.7–5.8 μm (Fig. 3), which show some differences compared with straw burning in the "heated kang". However, OC and K^+ displayed similar size distribution patterns to those produced by the "heated kang". OC levels in the size range 0.4–0.7 μm were about 1.6 times larger than those for sizes <0.4 μm, which are similar to those
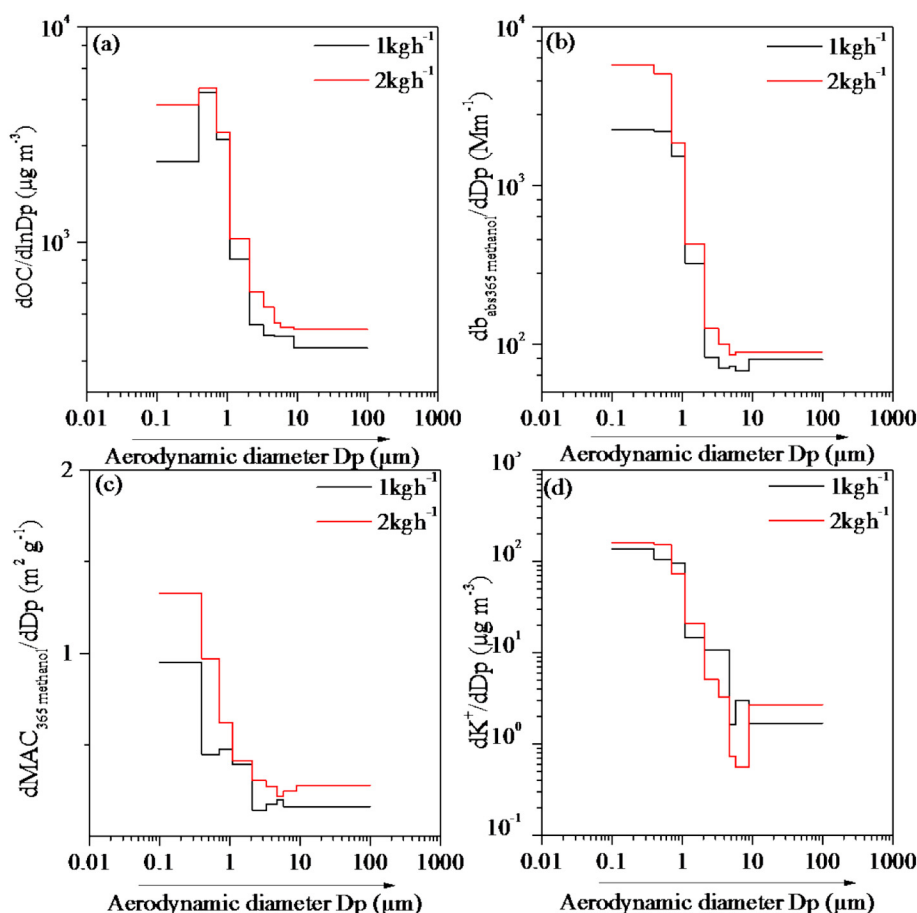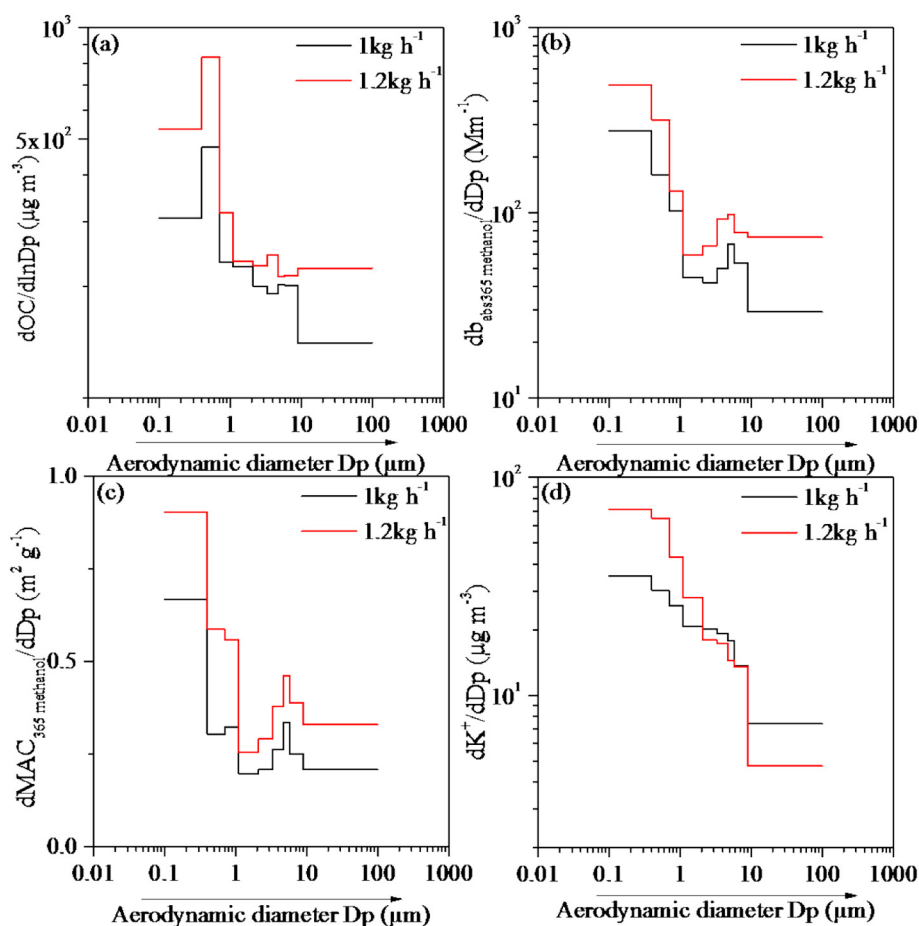

Fig. 2. Size distributions of (a) OC, (b) $b_{abs365,methanol}$, (c) $MAC_{365,methanol}$, and (d) K^+ from maize straw smoldering in the "heated kang" (1 kg h^{-1} & 2 kg h^{-1}).

Fig. 3. Size distributions of (a) OC, (b) $b_{abs365,methanol}$, (c) $MAC_{365,methanol}$, and (d) K^+ from maize straw smoldering in the advanced stove (1 kg h^{-1} & 1.2 kg h^{-1}).

obtained for the "heated kang". The $b_{abs365,methanol}$ value for sizes <0.4 μm was 277.4 Mm^{-1} in the advanced stove, which is a decrease of 87.6% relative to the "heated kang" for the same burning rate of 1 kg h^{-1}. The value of $MAC_{365,methanol}$ for sizes <0.4 μm was 0.95 m^2 g^{-1} in the "heated kang" and 0.67 m^2 g^{-1} in the advanced stove for the same burning rate of 1 kg h^{-1}. Burning rates also have little influence on the optical properties size distribution pattern in the advanced stove, but the optical properties values showed a clear diversity. For example, $b_{abs365,methanol}$ for sizes <0.4 μm and a burning rate of 1.2 kg h^{-1} was 489.0 Mm^{-1}, which is dramatically lower than the value 277.4 Mm^{-1} for the 1.0 kg h^{-1} rate, and MAC_{365} (<0.4 μm) also decreased from 0.9 m^2 g^{-1} to 0.7 m^2 g^{-1}. Thus, straw burning in a "heated kang" evidently emits more BrC with sizes <0.4 μm compared with briquette burning in an advanced stove.

3.4. BrC absorption properties in relation to organic and inorganic species

As discussed earlier, maize straw smoldering in a "heated kang" and straw briquette burning in an advanced stove are important emission sources of BrC. The relationships between $b_{abs365,methanol}$ and the OC, OC fractions, EC, and K^+ (biomass burning tracer) were investigated here to understand the characteristics of BrC emission sources.

K^+ was taken as a marker of biomass burning (Shen et al., 2009). In the present study, a strong correlation was found between $b_{abs365,methanol}$ and K^+ (Fig. S2), indicating that the importance of biomass burning to BrC particle production. In addition, the eight carbon fractions were characterized by the different emission sources. From our data, the correlation coefficient between $b_{abs365,methanol}$ with the four carbonic fractions followed a decreasing order as: OC1 (r = 0.94,
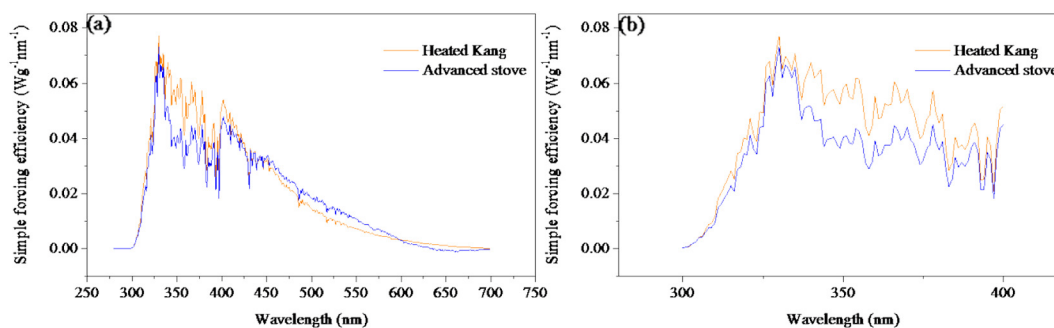

Fig. 4. Simple forcing efficiency of MSOC from PM$_{2.5}$ biomass burning samples integrated with the wavelength range of (a) 280–700 nm and (b) 300–400 nm under different combustion conditions.
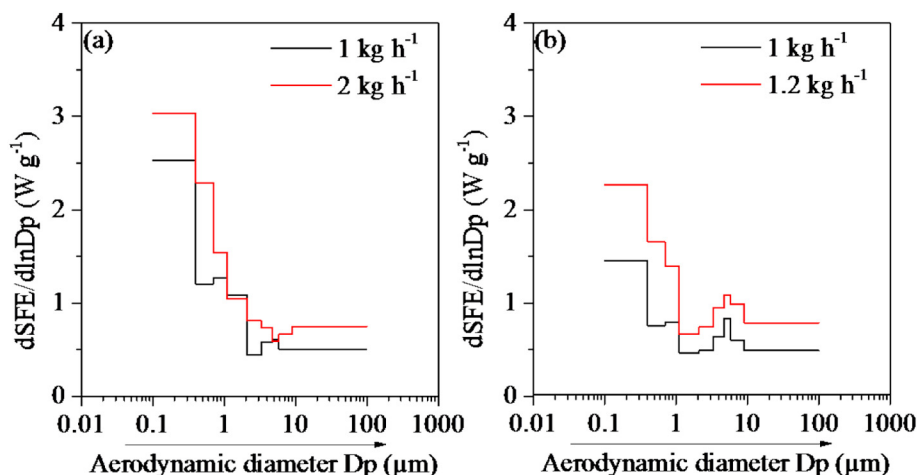
Fig. 5. Size distributions of SFE for MSOC integrated from 300 to 400 nm emitted from (a) "heated kang" and (b) advanced stove.

P < 0.0001), OC2 (r = 0.84, P < 0.0001), OC3 (r = 0.76, P < 0.0001), and OC4 (r = 0.52, P < 0.0001) (Fig. S3). OC1 and OC2 were produced at relative low temperatures in comparison with OC3 and OC4, and the organic matter that was composed of these two fractions was mostly semi-volatile OC (Chow et al., 2004). In the present study, the OC1 and OC2 levels from smoldering in the "heated kang" were much higher than those produced from burning in an advanced stove. Moreover, the value of $b_{abs365,methanol}$ for smoldering was much higher than that from burning in an advanced stove. Therefore, BrC were possibly emitted during the smoky, smoldering phase of the experiments when flames were hardly sighted and the temperature was relatively low. Considering the widespread use of "heated kangs" for winter heating in rural areas of the Guanzhong Plain, majority of $PM_{2.5}$ BrC can be attributed as arising from these smoldering processes (Shen et al., 2017a).

3.5. Evaluation of radiative forcing reduction

In this study, a simple model was used to estimate the climatic impact of methanol SOC. Fig. 4a shows the integrated absorption radiative forcing from 280 to 700 nm for biomass burning samples from the "heated kang" and the advanced stove. The average, integrated SFE values were thus estimated to be 8.3 W g^{-1} for smoldering in the "heated kang" and 7.7 W g^{-1} for briquette burning in the advanced stove, which indicates the importance of radiative forcing of absorption caused by biomass burning. It was noted that the SFE value from the advanced stove was 7.7% lower than that of the "heated kang". However, at UV wavelengths (300–400 nm), a near 20% reduction in the SFE value was observed from the "heated kang" relative to the advanced stove (Fig. 4b). The results highlight that maize straw briquette burning in an advanced stove can reduce the absorption radiative forcing more effectively at UV wavelengths compared to straw smoldering in a "heated kang".

The size distributions of the SFE values at UV wavelengths from both the "heated kang" and the advanced stove were also estimated (Fig. 5). The value of SFE for both the "heated kang" and the advanced stove showed similar size distributions pattern as those of the $MAC_{365,methanol}$ size distributions mentioned earlier. Burning rates influenced little on the SFE size distribution patterns, but the values showed some differences. For the "heated kang", the SFE value for sizes <0.4 μm and a burning rate of 1 kg h^{-1} was 2.5 W g^{-1}, which increased to 3.0 W g^{-1} for 2 kg h^{-1}. For the advanced stove, the values changed from 1.4 W g^{-1} (1 kg h^{-1}) to 2.3 W g^{-1} (1.2 kg h^{-1}). Such results imply that a faster burning rate may lead to higher absorption radiative forcing. Therefore, using an advanced stove can reduce the absorption of solar radiation of MSOC comparing to the "heated kang" at UV wavelengths.

4. Conclusions

This study investigated the light absorption of BrC in aerosol extracts from straw smoldering burning in a "heated kang" and briquettes in an advanced stove. The correlation between OC and $b_{abs365,methanol}$ was strong from the biomass burning source samples (r of 0.96 compared to 0.60 for EC), which illustrates that BrC is a significant component in OC. The values of $b_{abs365,methanol}$ correlated better with OC1 than OC2, OC3 and OC4, indicating that BrC was mainly produced by low temperature combustion of biomass burning.

Comparison of b_{abs365} between the methanol and water soluble extracts illustrated that a larger portion of BrC absorption was extracted by methanol. The size distribution results showed that there were some differences in the light absorption and compounds peaks with respect to the different combustion conditions. For smoldering straw in the "heated kang", $b_{abs365,methanol}$, $MAC_{365,methanol}$, and K^+ peaked at sizes <0.4 μm, while OC tended to be larger (0.4–0.7 μm). In contrast, the $b_{abs365,methanol}$ and $MAC_{365,methanol}$ values for the briquettes in an advanced stove displayed an additional, minor peak for sizes of 4.7–5.8 μm. The proportion (<0.4 μm) of $b_{abs365,methanol}$ produced by the advanced stove varied little for different burning rates. The differences in the proportions (<0.4 μm/ 0.4–0.7 μm) between OC and $b_{abs365,methanol}$ suggest that BrC is predominately produced as finer particles (<0.4 μm). The advanced stove can reduce the SFE value by nearly 20% in UV bands compared to the "heated kang". Finally, an advanced stove with a higher MCE could be a positive countermeasure to reduce BrC emission during the heating season in the Guanzhong Plain.

Appendix A. Supplementary data

Supplementary data to this article can be found online at https://doi.org/10.1016/j.scitotenv.2017.11.353.

References

Andreae, M.O., Merlet, P., 2001. Emission of trace gases and aerosols from biomass burning. Global. Biogeochem. Cy. 15 (4), 955–966.

Andreae, M.O., Gelencser, A., 2006. Black carbon or brown carbon? The nature of light-absorbing carbonaceous aerosols. Atmos. Chem. Phys. 6 (10), 3131–3148.

Bahadur, R., Praveen, P.S., Xu, Y., Ramanathan, V., 2012. Solar absorption by elemental and brown carbon determined from spectral observations. PNAS 109 (43), 17366–17371.

Bond, T.C., Bergstrom, R.W., 2006. Light absorption by carbonaceous particles: an investigative review. Aerosol Sci. Technol. 40 (1), 27–67.

Cao, J.J., Lee, S.C., Ho, K.F., Zhang, X.Y., Zou, S.C., Fung, K., Chow, J.C., Watson, J.G., 2003. Characteristics of carbonaceous aerosol in Pearl River Delta Region, China during 2001 winter period. Atmos. Environ. 37, 1451–1460.

Cao, J.J., Wu, F., Chow, J.C., Lee, S.C., Li, Y., Chen, S.W., An, Z.S., Fung, K.K., Watson, J.G., Zhu, C.S., Liu, S.X., 2005. Characterization and source apportionment of atmospheric organic and elemental carbon during fall and winter of 2003 in Xi'an, China. Atmos. Chem. Phys. 5, 3127–3137.

Chen, Y., Bond, T.C., 2010. Light absorption by organic carbon from wood combustion. Atmos. Chem. Phys. 10 (4), 1773–1787.

Cheng, Y., He, K.B., Du, Z.Y., Engling, G., Liu, J.M., Ma, Y.L., Zheng, M., Weber, R.J., 2016. The characteristics of brown carbon aerosol during winter in Beijing. Atmos. Environ. 127, 355–364.

Chow, J.C., Watson, J.G., Kuhns, H., Etyemezian, V., Lowenthal, D.H., Crow, D., Kohl, S.D., Engelbrecht, J.P., Green, M.C., 2004. Source profiles for industrial, mobile and area sources in the Big Bend Regional Aerosol Visibility and Observational study. Chemosphere 54, 185–208.

Chung, C.E., Ramanathan, V., Decremer, D., 2012. Observationally constrained estimates of carbonaceous aerosol radiative forcing. PNAS 109 (29), 11624–11629.

Chylek, P., Wong, J., 1995. Effect of absorbing aerosol on global radiation budget. Geophys. Res. Lett. 22, 929–931.

Feng, Y., Ramanathan, V., Kotamarthi, V.R., 2013. Brown carbon: a significant atmospheric absorber of solar radiation. Atmos. Chem. Phys. Discuss. 13, 2795–2833.

Hecobian, A., Zhang, X., Zheng, M., Frank, N., Edgerton, E.S., Weber, R.J., 2010. Water-Soluble Organic Aerosol material and the light-absorption characteristics of aqueous extracts measured over the Southeastern United States. Atmos. Chem. Phys. 10, 5965–5977.

Hoffer, A., Gelencser, A., Guyon, P., Kiss, G., Schmid, O., Frank, G.P., Artaxo, P., Andreae, M.O., 2006. Optical properties of humic-like substances (HULIS) in biomass-burning aerosols. Atmos. Chem. Phys. 6, 3563–3570.

Kirchstetter, T.W., Novakov, T., Hobbs, P.V., 2004. Evidence that the spectral dependence of light absorption by aerosols is affected by organic carbon. J. Geophys. Res. 109, D21208.

Lack, D.A., Langridge, J.M., Bahreini, R., 2012. Brown carbon and internal mixing in biomass burning particles. PNAS 109 (37), 14802–14807.

Lambe, A.T., Cappa, C.D., Massoli, P., Onasch, T.B., Forestieri, S.D., Martin, A.T., Cummings, M.J., Croadale, D.R., Brune, W.H., Worsnop, D.R., Davidovits, P., 2013. Relationship between oxidation level and optical properties of secondary organic aerosol. Environ. Sci. Technol. 47 (12), 6349–6357.

Laskin, A., Laskin, J., Nizkorodov, S.A., 2015. Chemistry of atmospheric brown carbon. Chem. Rev. 115 (10), 4335–4382.

Liu, J., Bergin, M., Guo, H., King, L., Kotra, N., Edgerton, E., Weber, R.J., 2013. Size-resolved measurements of brown carbon in water and methanol extracts and estimates of their contribution to ambient fine-particle light absorption. Atmos. Chem. Phys. 13, 12389–12404.

Lukacs, H., Gelencser, A., Hammer, S., Puxbaum, H., Pio, C., Legrand, M., Kasper-Giebl, A., Handler, M., Limbeck, A., Simpson, D., Preunkert, S., 2007. Seasonal trends and possible sources of brown carbon based on 2-year aerosol measurements at six sites in Europe. J. Geophys. Res. 112 (D23), 4789–4797.

Oanh, N.T.K., Ly, B.T., Tipayarom, D., Manandhar, B.R., Prapat, P., Simpson, C.D., Liu, L.J., 2011. Characterization of particulate matter emission from open burning of rice straw. Atmos. Environ. 45 (2), 493.

Poschl, U., 2003. Aerosol particle analysis: challenges and progress. Anal. Bioanal. Chem. 375 (1), 30–32.

Shen, Z.X., Arimoto, R., Cao, J.J., Zhang, R.J., Li, X.X., Du, N., Okuda, T., Nakao, S., Tanaka, S., 2008. Seasonal variations and evidence for the effectiveness of pollution controls on water-soluble inorganic species in total suspended particulates and fine particulate matter from Xi'an, China. J. Air Waste Manage. Assoc. 58, 1560–1570.

Shen, Z.X., Cao, J.J., Arimoto, R., Han, Z.W., Zhang, R.J., Han, Y.M., Liu, S.X., Okuda, T., Nakao, S., Tanaka, S., 2009. Ionic composition of TSP and PM$_{2.5}$ during dust storms and air pollution. Atmos. Environ. 43, 2911–2918.

Shen, G.F., Wang, W., Yang, Y.F., Ding, J.N., Xue, M.A., Min, Y.J., Zhu, C., Shen, H.Z., Li, W., Wang, B., Wang, R., Wang, L., Tao, S., Russell, A.G., 2011. Emissions of PAHs from indoor crop residue burning in a typical rural stove: emission factors, size distributions, and gas-particle partitioning. Environ. Sci. Technol. 45, 1206–1212.

Shen, Z.X., Zhang, Q., Cao, J.J., Zhang, L.M., Lei, Y.L., Huang, Y., Huang, R.J., Gao, J.J., Zhao, Z.Z., Zhu, C.S., Yin, X.L., Zheng, C.L., Xu, H.M., Liu, S.X., 2017a. Optical properties and possible sources of brown carbon in PM$_{2.5}$ over Xi'an, China. Atmos. Environ. 150, 322–330.

Shen, Z.X., Lei, Y.L., Zhang, L.M., Zhang, Q., Zeng, Y.L., Tao, J., Zhu, C.S., Cao, J.J., Xu, H.M., Liu, S.X., 2017b. Methanol extracted brown carbon in PM$_{2.5}$ over Xi'an, China: seasonal variation of optical properties and sources identification. Aerosol. Sci. Eng. 1–9.

Srinivas, B., Sarin, M.M., 2014. Brown carbon in atmospheric outflow from the Indo-Gangetic Plain: mass absorption efficiency and temporal variability. Atmos. Environ. 89, 835–843.

Sun, J., Shen, Z.X., Cao, J.J., Zhang, L.M., Wu, T.T., Zhang, Q., Yin, X.L., Lei, Y.L., Huang, Y., Huang, R.J., Liu, S.X., Han, Y.M., Xu, H.M., Zheng, C.L., Liu, P.P., 2017. Particulate matters emitted from maize straw burning for winter heating in rural areas in Guanzhong Plain, China: current emission and future reduction. Atmos. Res. 184, 66–76.

Wang, G.H., Chen, C.L., Li, J.J., Zhou, B.H., Xie, M.J., Hu, S.Y., Kawamura, K., Chen, Y., 2011. Molecular composition and size distribution of sugars, sugar-alcohols and carboxylic acids in airborne particles during a severe urban haze event caused by wheat straw burning. Atmos. Environ. 45, 2473–2479.

Wang, X., Heald, C.L., Ridley, D.A., Schwarz, J.P., Spackman, J.R., Perring, A.E., Coe, H., Liu, D., Clarke, A.D., 2014. Exploiting simultaneous observational constraints on mass and absorption to estimate the global direct radiative forcing of black carbon and brown carbon. Atmos. Chem. Phys. 14 (11), 17527–17583.

Washenfelder, R.A., Attwood, A.R., Brock, C.A., Guo, H., Xu, L, Weber, R.J., Ng, N.L., Allen, H.M., Ayres, B.R., Baumann, K., Cohen, R.C., Draper, D.C., Duffey, K.C., Edgerton, E., Fry, J.L., Hu, W.W., Jmienez, J.L., Palm, B.B., Romer, P., Stone, E.A., Wooldridge, P.J., Brown, S.S., 2015. Biomass burning dominates brown carbon absorption in the rural southeastern United States. Geophys. Res. Lett. 42 (2), 653–664.

Yan, C., Zheng, M., Sullivan, A.P., Bosch, C., Desyaterik, Y., Andersson, A., Li, X.Y., Guo, X.S., Zhou, T., Gustafsson, O., Jeffrey, L.C.J., 2015. Chemical characteristics and light-absorbing property of water-soluble organic carbon in Beijing: biomass burning contributions. Atmos. Environ. 121, 4–12.

Yang, M., Howell, S.G., Zhuang, J., Huebert, B.J., 2009. Attribution of aerosol light absorption to black carbon, brown carbon, and dust in China–interpretations of atmospheric measurements during EAST-AIRE. Atmos. Chem. Phys. 8 (3), 10913–10954.

Zhang, X.L., Lin, Y.H., Surratt, J.D., Weber, R.J., 2013. Sources, composition and absorption Angström exponent of light-absorbing organic components in aerosol extracts from the Los Angeles Basin. Environ. Sci. Technol. 47, 3685–3693.

Zhang, T., Cao, J.J., Chow, J.C., Shen, Z.X., Ho, K.F., Ho, S.S.H., Liu, S.X., Han, Y.M., Watson, J.G., Wang, G.H., Huang, R.J., 2014. Characterization and seasonal variations of levoglucosan in fine particulate matter in Xi'an, China. J. Air Waste Manage. Assoc. 64 (11), 1317–1327.

Zhao, R., Lee, A.K.Y., Huang, L., Li, X., Yang, F., Abbatt, J.P.D., 2015. Photochemical processing of aqueous atmospheric brown carbon. Atmos. Chem. Phys. 15 (2), 2957–2996.

Zhu, C.S., Cao, J.J., Tsai, C.J., Shen, Z.X., Liu, S.X., Huang, R.J., Zhang, N.N., Wang, P., 2016. The rural carbonaceous aerosols in coarse, fine, and ultrafine particles during haze pollution in northwestern China. Environ. Sci. Pollut. Res. 23, 4569–4575.